

# Microsegregation and precipitates of an as-cast Co-based superalloy—microstructural characterization and phase stability modelling

J. Koßmann<sup>1</sup> · C. H. Zenk<sup>2</sup> · I. Lopez-Galilea<sup>3</sup> · S. Neumeier<sup>2</sup> · A. Kostka<sup>4</sup> · S. Huth<sup>3</sup> · W. Theisen<sup>3</sup> · M. Göken<sup>2</sup> · R. Drautz<sup>1</sup> · T. Hammerschmidt<sup>1</sup>

Received: 31 December 2014 / Accepted: 10 June 2015 / Published online: 23 June 2015  
© Springer Science+Business Media New York 2015

**Abstract** The demand for increased efficiency of industrial gas turbines and aero engines drives the search for the next generation of materials. Promising candidates for such new materials are Co-based superalloys. We characterize the microsegregation and solidification of a multi-component Co-based superalloy and compare it to a ternary Co–Al–W compound and to two exemplary Ni-based superalloys by combining the experimental characterization of the as-cast microstructures with complementary modelling of phase stability. On the experimental side, we characterize the microstructure and precipitates by electron microscopy and energy-dispersive X-ray spectroscopy and determine the element distributions and microsegregation coefficients by electron probe microanalysis (EPMA). On the modelling side, we carry out solidification simulations and a structure map analysis in order to relate the local chemical composition with phase stability. We find that the microsegregation coefficients for the individual elements are very similar in the investigated Co-based and Ni-based

superalloys. By interpreting the local chemical composition from EPMA with the structure map, we effectively unite the set of element distribution maps to compound maps with very good contrast of the dendritic microstructure. The resulting compound maps of the microstructure in terms of average band filling and atomic-size difference explain the formation of topologically close-packed phases in the interdendritic regions. We identify B2, C14, and D0<sub>24</sub> precipitates with chemical compositions that are in line with the structure map.

## Introduction

Single-crystal Ni-based superalloys are a widely established class of materials for high-temperature applications, like turbine blades in industrial gas turbines or aero engines [1]. These materials exhibit good mechanical stability even at high temperatures due to their characteristic  $\gamma/\gamma'$ -microstructure [2]. The cuboidal  $\gamma'$ -precipitates of L1<sub>2</sub>–Ni<sub>3</sub>Al coexist with a matrix of a disordered  $\gamma$ -phase on a coherent A1 crystal lattice. In 2006 Sato et al. observed a similar microstructure in the ternary Co–Al–W system with L1<sub>2</sub>–Co<sub>3</sub>(Al,W)  $\gamma'$ -precipitates in the  $\gamma$ -phase [3]. Since then, Co-based single-crystal superalloys are studied as candidates for the next generation of high-temperature superalloys. In particular it was shown that Co–Al–W-based superalloys exhibit flow-stress anomalies similar to Ni-based superalloys [4, 5]. Systematic screenings demonstrated that critical material parameters like, e.g. the  $\gamma'$  volume fraction, characteristic phase transformation temperatures, and creep strength can be adjusted by alloying to reach the quality of Ni-based superalloys [6–8].

In our recent publication [9] the heat treatment of the complex Co-based superalloy ERBOCo-0 was discussed.

---

**Electronic supplementary material** The online version of this article (doi:10.1007/s10853-015-9177-8) contains supplementary material, which is available to authorized users.

---

✉ J. Koßmann  
joerg.kossmann@rub.de

<sup>1</sup> ICAMS, Ruhr-Universität Bochum, Bochum, Germany

<sup>2</sup> Lehrstuhl I: Allgemeine Werkstoffeigenschaften, Friedrich-Alexander-Universität Erlangen-Nürnberg, Erlangen, Germany

<sup>3</sup> Lehrstuhl Werkstofftechnik, Ruhr-Universität Bochum, Bochum, Germany

<sup>4</sup> Max-Planck-Institut für Eisenforschung GmbH, Düsseldorf, Germany

In the current work, ERBOCo-0 is further investigated and compared to the simple Co–Al–W ternary system ERBOCo-9W and the two Ni-based superalloys ERBO-1 and Astra2-W. All four alloys were characterized in the as-cast state by a combination of experimental and theoretical techniques with regard to microsegregation, solidification, and microstructure. The experimental metallurgy was complemented by an analysis with a recently derived structure map [10] for topologically close-packed (TCP) phases. Understanding the formation of TCP phases (for a review see e.g. Ref. [11]) is of great importance for alloy development as they reduce the  $\gamma/\gamma'$ -hardening effect and lead to a depletion of strengtheners in the  $\gamma$ -matrix [12, 13]. We interpret the precipitation of intermetallic phases by analysing local chemical compositions with the structure map and verify our findings with the corresponding transmission electron microscopy (TEM) measurements.

In “Materials and methodology” section we introduce the investigated superalloys as well as our experimental and theoretical methodology. The experimentally observed microsegregation is discussed and interpreted in terms of the structure map in “Microsegregation” section. In “Precipitates in as-cast ERBOCo-0” section the observed intermetallic precipitates in ERBOCo-0 are described and compared to predictions of solidification path modelling. Our findings are summarized in “Conclusions” section.

## Materials and methodology

### Materials

The nominal chemical compositions of all investigated materials are given in Table 1. ERBO-1 is a 2nd generation single-crystal Ni-based superalloy similar to the commercial CMSX-4 and was provided by Doncasters Precision Casting, Bochum, Germany in the as-cast state. Astra2-W is an experimental W-rich 1st generation Ni-based superalloy which has been investigated for comparison with the W-rich Co-based superalloys. ERBOCo-9W is a single-crystal ternary Co–Al–W alloy while ERBOCo-0 is a multi-component

Co-based superalloy. The latter three were developed and cast as single-crystals using the Bridgman process at the University of Erlangen-Nürnberg, Germany. The hot melt at 1560 °C was poured into the moulding tray which was then pulled out of the furnace with a removal speed of 3 mm/min. The average dendrite arm spacing is 220  $\mu\text{m}$  for ERBOCo-0, 250  $\mu\text{m}$  for ERBOCo-9W, and 260  $\mu\text{m}$  for the Astra2-W sample. The bar diameter is 11 mm for Astra-2W and 12 mm for the other samples.

### Microstructural characterization

The samples for scanning electron microscopy (SEM), energy-dispersive spectroscopy (EDS), and electron probe microanalysis (EPMA) were cut perpendicular to the [001]-direction, mounted in epoxy and mechanically polished to mirror finish without etching. The microstructure was investigated using an SEM Zeiss (LEO) 1530 VP with 8.5 mm working distance and an acceleration voltage of 20 kV for a secondary electron micrograph (SEM) as well as for a back-scattered electron (BSE) micrograph. TEM experiments were performed with a Jeol JEM-2200FS operated at 200 kV with STEM high-angle annular dark field (HAADF) detector and EDAX EDX system. The specimens were prepared from regions of interest along the matrix/TCP interface using a Jeol JEM-9320 focused ion beam (FIB) system at 30 kV. To measure segregation on a dendritic scale EPMA mappings were performed with a Jeol JXA-8100 instrument. The composition was measured for each mapping point, i.e. 200  $\times$  200 points for the three ERBO alloys and 300  $\times$  300 points for Astra2-W. Using probe sizes of 5  $\mu\text{m}$  for the former three alloys and 2.5  $\mu\text{m}$  for the latter corresponding to characterized areas of 1 mm  $\times$  1 mm and 0.75 mm  $\times$  0.75 mm, respectively.

### Structure map

The employed structure map for TCP phases introduced by Seiser, Drautz, and Pettifor (SDP structure map) [10] describes the structural stability of TCP phases in a compound by making use of atomic properties of the alloying elements.

**Table 1** Nominal composition of the investigated single-crystal Co–Al–W alloy ERBOCo-9W, the multi-component Co-based superalloy ERBOCo-0, and the CMSX-4 alike ERBO-1 and W-rich Astra2-W Ni-based superalloy

	(at.%)										
	Ni	Co	Cr	W	Al	Ti	Ta	Hf	Mo	Re	Si
ERBOCo-9W	–	82.00	–	9.00	9.00	–	–	–	–	–	–
ERBOCo-0	20.00	56.50	6.00	5.00	8.00	2.50	1.50	0.10	–	–	0.40
ERBO-1	62.95	10.01	7.48	2.12	12.62	1.27	2.18	0.03	0.38	0.96	–
Astra2-W	65.70	9.00	6.00	3.60	13.50	–	2.20	–	–	–	–

These are combined with the chemical composition of the compound in terms of the average valence band filling

$$\bar{N} = \sum_i c_i N_i \tag{1}$$

and the relative volume difference

$$\frac{\Delta V}{\bar{V}} = \sum_{ij} c_i c_j \frac{\Delta V_{ij}}{\bar{V}_{ij}} = \sum_{ij} c_i c_j \frac{|V_i - V_j|}{\frac{1}{2}(V_i + V_j)} \tag{2}$$

as coordinates of the structure map. Here,  $c_i$  is the molar fraction,  $N_i$  the effective number of valence electrons, and  $V_i$  is the atomic volume (computed from the metallic radii [14–17]) of the alloying element  $i$ . The relative volume difference  $\Delta V/\bar{V}$  is computed from the atomic volume differences  $\Delta V_{ij}$  and the average atomic volumes  $\bar{V}_{ij}$  in order to quantify the atomic-size differences in the alloy. It increases with the differences in the atomic volumes of the alloying elements and takes a value of zero for pure unaries. It has been shown [10] that the structure map distinguishes the different TCP phases in terms of distinct stability windows, indicated as polyhedra in Fig. 1, that contain the respective experimentally observed binary and multi-component TCP phases [10]. The influence of  $\bar{N}$  on the relative structural stability of TCP phases is well known from the calculations with density functional theory (DFT) [18, 19] and approximate electronic structure methods [20–23]. The interplay of  $\bar{N}$  and  $\Delta V/\bar{V}$  was discussed in DFT calculations for various binary systems [22–25].

So far the structure map has been applied to single-phase compound systems, in this work we apply it to precipitates and multi-phase compound systems using the local chemical

compositions. In the current work, we additionally considered the B2 (CsCl),  $L1_2$  ( $\gamma'$ ), and  $D0_{24}$  ( $\eta$ -Ni<sub>3</sub>Ti) structures that are relevant for Ni- and Co-based single-crystal superalloys. These phases were included in the structure map by considering the compositions of all binary and ternary pure d-block compounds with these structures according to the Pearson database [25], see Fig. 1. The region of the  $D0_{24}$  structure (relevant for ERBOCo-0, see “Microsegregation” and “Precipitates in as-cast ERBOCo-0” sections) is rather small and well separated from the TCP windows in the structure map. The  $L1_2$  and B2 regions show a rather large variety of band filling and relative volume difference and hence overlap with all other TCP phase windows. In Online Resource 1, we compiled further applications of the structure map to commercially available Co- and Ni-based superalloys and composition variations.

### Thermodynamic calculations

The CALPHAD method [26, 27] was applied to predict the stability, volume fraction, and composition of phases for the investigated alloys using the software package ThermoCalc™ version 5 [28]. The database TCNi5 [29], developed for Ni-based superalloys, was used for all four alloys, i.e. also for the investigated Co-based materials. We expect limitations for complex Co-based materials and apply it mainly to identify the range of applicability.

### Microsegregation

### SEM and EPMA experiments

The investigated Co- and Ni-based superalloys have as-cast microstructures with a fourfold dendrite symmetry normal

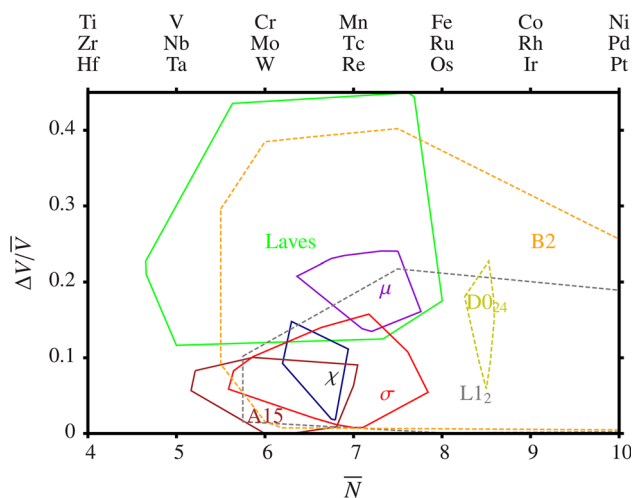


**Fig. 1** Structure map with average valence band filling  $\bar{N}$  and relative volume difference  $\Delta V/\bar{V}$  (Eqs. 1, 2) The coloured polyhedra mark the regions of phase stability for TCP phases [10] as well as  $L1_2$ ,  $D0_{24}$ , and B2 structures. Transition-metal elements corresponding to  $\bar{N}$  are indicated

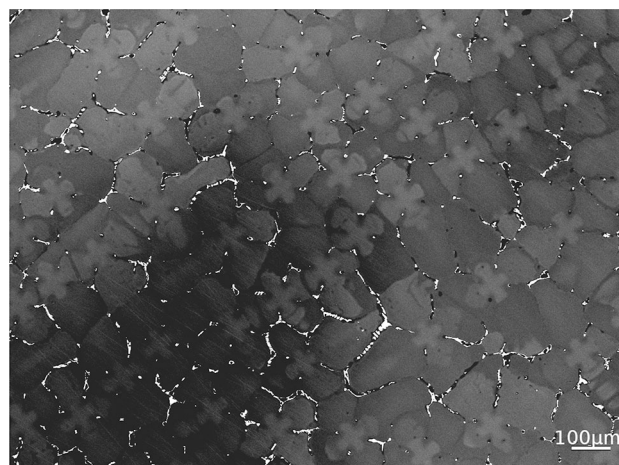


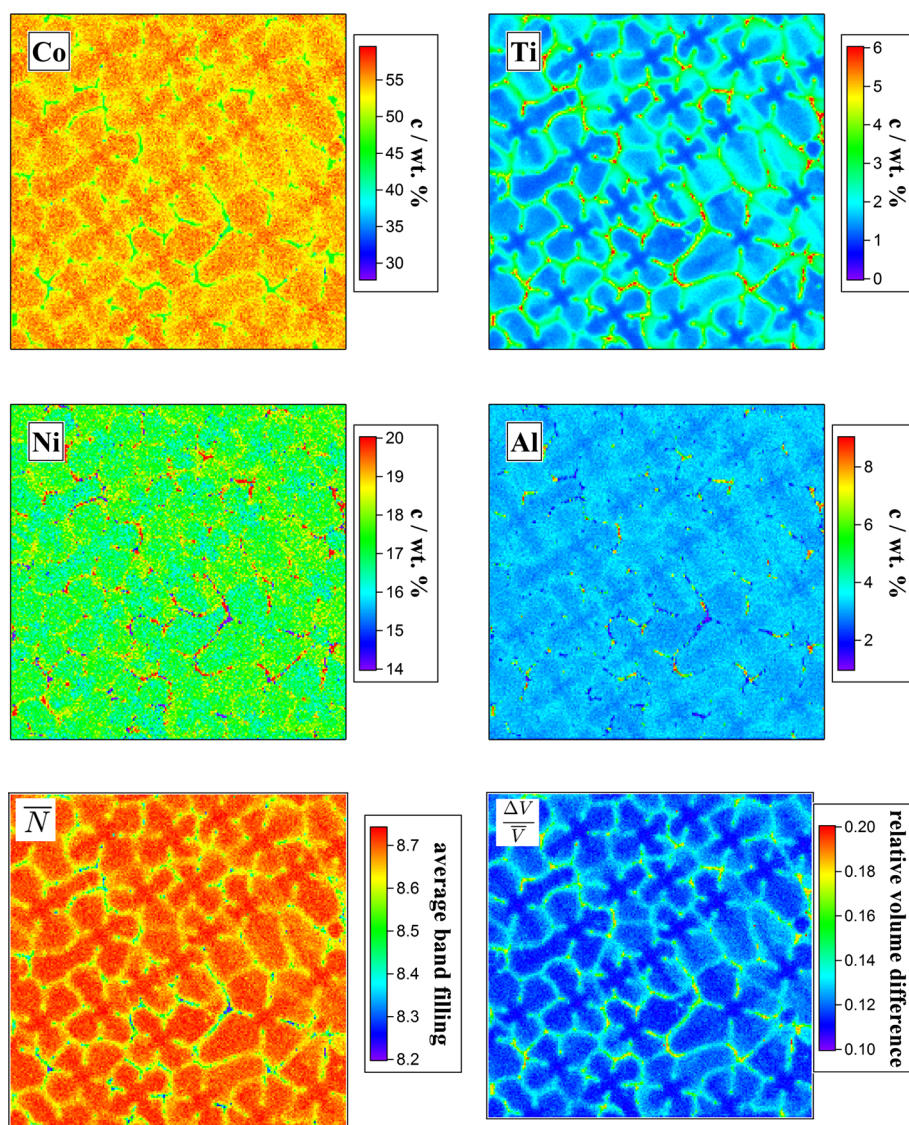
**Fig. 2** SEM (BSE) micrograph of the as-cast microstructure of the Co-based superalloy ERBOCo-0

to the [001] growth direction. Figure 2 shows a SEM (BSE) micrograph of the as-cast ERBOCo-0 sample normal to the [001] axis. The main differences between the as-cast microstructures of the studied alloys are the microsegregation and the intermetallic precipitates observed in the interdendritic regions. In order to quantify the microsegregation during casting, all four alloys were characterized by EPMA measurements. For the case of ERBOCo-0, the element distribution maps of Co, Ti, Ni, and Al are shown in Fig. 3 (Further EPMA results have been published in Ref. [9]). These indicate that Cobalt segregates to the dendrite core (DC) while Titanium, Nickel, and Aluminium segregate to the interdendritic regions (IR).

In order to determine the microsegregation coefficient for each element, we use a statistical technique that was originally applied for binary alloys [30] and later adapted to multi-component Ni-based [31] and Co-based [32]

superalloys. In this procedure the EPMA measured element concentrations in the solid  $c_S$  are sorted in ascending order on the basis of their solid fraction  $f_S$ . *I.e.* the concentration data points from the DC, which solidifies at first, are assigned to  $f_S = 0$ , while the concentrations from the IR, which solidifies last, are assigned to  $f_S = 1$ . In Ref. [31] the data points were sorted in ascending order according to the difference in the concentration of Ta and Re,  $c_S(\text{Ta}) - c_S(\text{Re})$ , since this value increases continuously from the beginning to the end of solidification. In this work the Co mass fraction was used for sorting the element concentrations. This choice is motivated by (1) the monotonic decrease of Co during solidification, (2) the minimization of experimental scatter due to the high amount of Co, and (3) the presence of Co in all investigated alloys. The resulting concentrations are fitted to the Scheil–Gulliver equation under the assumption that diffusion

**Fig. 3** EPMA maps for the concentration of the elements Co, Ti, Ni, and Al in ERBOCo-0 and corresponding structure map coordinates  $\bar{N}$  and  $\Delta V/\bar{V}$  according to Eqs. 1 and 2. The maps for W, Cr, Ta, Hf, and Si have been published in Ref. [9]



during solidification and subsequent cooling is negligible up to the point where a splitting of the concentration curves is observed (see Fig. 4):

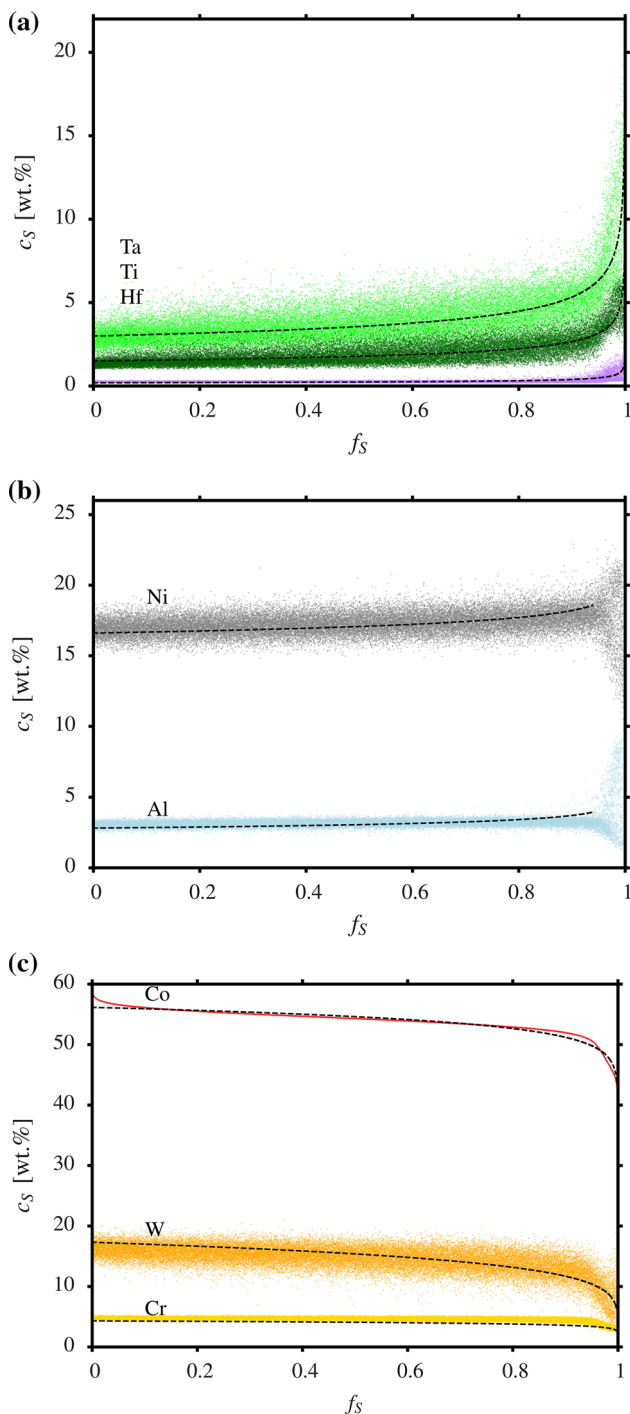


**Fig. 4** Solid compositions  $c_s$  in wt% for ERBOCo-0 obtained by EPMA as functions of solid fraction  $f_s$  (Eq. 3). Concentration profiles of (a) Ta (green), Ti (dark green), and Hf (magenta); b Ni (grey) and Al (blue); c Co (red), W (orange), and Cr (yellow). The black curves represents the Scheil–Gulliver fit according to Eq. 3 (Color figure online)

$$c_s = kc_0(1 - f_s)^{k-1} \tag{3}$$

Here,  $c_s$  and  $c_0$  are the element concentration (in wt%) in the solid and in the nominal composition, respectively;  $f_s$  the corresponding solid fraction and  $k$  the distribution coefficient. The sorted concentration values for Ta, Ti, Hf, Ni, Al, Co, W, and Cr in ERBOCo-0 (Fig. 4) are consistent with the EPMA maps that show Co, W, and Cr enrichment in the DC as well as Ta, Ti, and Hf enrichment in the IR. Al and Ni show a splitting in concentration towards the end of the solidification process at about  $f_s = 94\%$ . This corresponds to the solidification of the remaining melt in the IR and an associated formation of different phases. Consequently, the data points for  $f_s = 94\%$  have not been used for computing the microsegregation coefficients of ERBOCo-0.

The obtained microsegregation coefficients for all investigated alloys are shown in Fig 5. The microsegregation coefficients were found to be rather close to 1 in the simple ternary Co-alloy ERBOCo-9W since the degree of microsegregation is the lowest. This is in line with Ref. [32]. In the more complex Co-based superalloy ERBOCo-0, the considered elements show a very similar behaviour as in the Ni-based superalloys ERBO-1 and Astra2-W: Cr, Co, and W (as well as Mo and Re for ERBO-1) segregate preferably to the DC, whereas Ta, Ti, Al, and Ni segregate to the IR. The computed microsegregation coefficients in ERBO-1 are in good agreement with previous studies

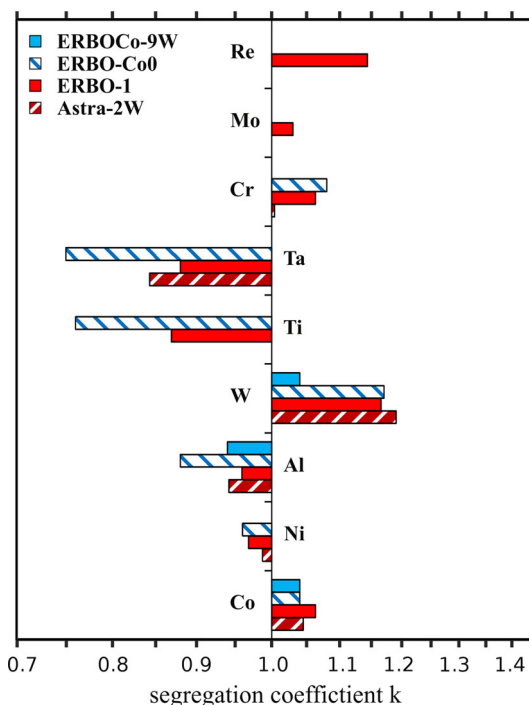


**Fig. 5** Microsegregation Coefficients for all investigated alloys. Hf and Si are not shown here due to the weak resolution caused by the low mass fractions

[33–35], except for W and Re, for which much larger  $k$  values (up to 1.6) have been reported. This difference can result from the different casting conditions of the samples. The microsegregation of Ta to the IR is more pronounced in ERBOCo-0 compared to the two Ni-based superalloys, in line with previous findings [32]. This might improve the castability, because it would take account for convective instabilities during casting that are caused by density fluctuations due to heavy elements segregating to the dendrite cores. The observed similarities in the microsegregation behaviour suggest that local enrichments of elements in Co-based superalloys can be as high as in Ni-based superalloys.

### Interpretation with structure map

The spatially resolved local chemical composition from the EPMA experiments can be directly linked to the structure map. Therefore the values of  $\bar{N}$  and  $\Delta V/\bar{V}$  for each point of the microstructure segment were computed using the local chemical composition from EPMA. The resulting representation of the elemental distribution in terms of  $\bar{N}$  and  $\Delta V/\bar{V}$  effectively unites the set of element distribution maps. The resulting compound map reflects the dendritic microstructure of ERBOCo-0 with very good contrast (see Fig. 3). The dendritic cores are characterized by values of  $\Delta V/\bar{V}$  and  $\bar{N}$  close to the values of the nominal compositions of the alloys. In the interdendritic regions, however, the value of  $\bar{N}$  is considerably reduced from the nominal value of the alloy, while  $\Delta V/\bar{V}$  is increased by nearly a factor of two. These differences can be attributed to the increase in Ta, Ti, Hf, and the decrease of Co and W (compare with Fig. 4a, c).

The EPMA results of the as-cast dendritic microstructure can be further analysed by making use of the value of solid fraction for the different points in the microstructure. Following the chemical compositions along the variation of the solid fractions  $f_s$  from 0 to 1 effectively corresponds to following the solidification path. Therefore, by computing the values of  $\bar{N}$  and  $\Delta V/\bar{V}$  for all compositions at each value of  $f_s$ , one can follow the solidification path in the structure map along the variation of  $f_s$  as shown in Fig. 6.

With increasing  $f_s$  the volume difference is increased and a lower band filling can be observed, which effectively shifts the corresponding positions in the structure map closer to the TCP phase regions. Especially the enrichment of Ti, Ta, and Hf in the IR shifts the local compositions towards the TCP phase regions. In fact, several regions in the microstructure exhibit compositions that are located in the stability regions of the TCP phases. From this, one would already expect an increased likelihood of Laves or  $\mu$  phase formation and indeed these data points can be

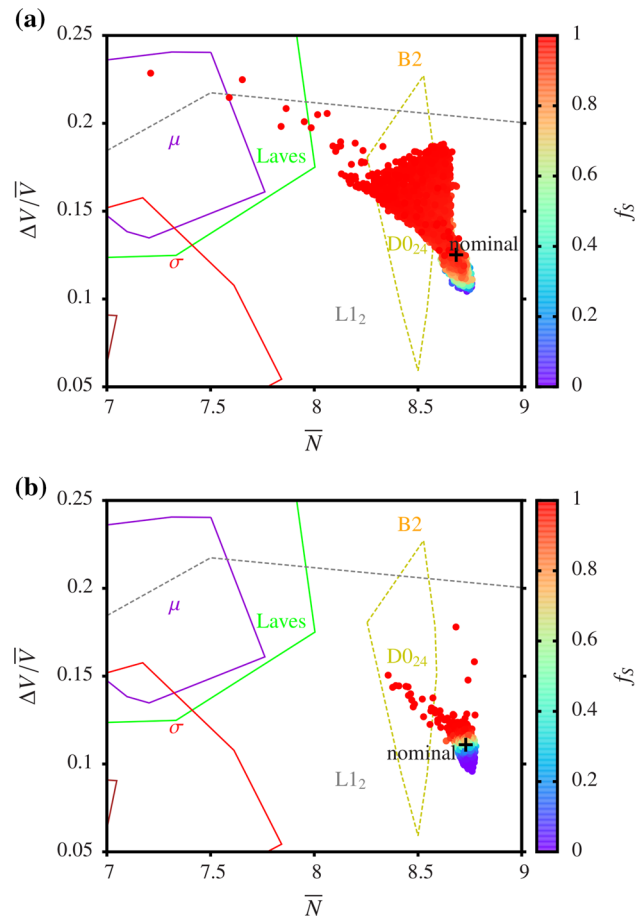


**Fig. 6** Structure map analysis of chemical compositions from EPMA for **a** ERBOCo-0 and **b** ERBOCo-9W. The variation during solidification is indicated by ordering the measured compositions according to increasing solid fraction  $f_s$

assigned to such precipitates as discussed in “Precipitates in as-cast ERBOCo-0” section. For comparison the same analysis was carried out for the case of ERBOCo-9W (Fig. 6b). Here, the same trend of increasing  $\Delta V/\bar{V}$  and decreasing  $\bar{N}$  during solidification can be observed. However, due to weaker microsegregation, the dendritic structure is less pronounced and the TCP phase regions in the structure map are not reached. This is consistent with the absence of TCP phase precipitates in the experiments.

### Precipitates in as-cast ERBOCo-0

#### Electron microscopy experiments

The microsegregation during casting discussed in the previous sections is responsible for heterogeneities and precipitation of secondary phases. The formation of these phases takes place towards the end of the solidification

process, therefore these phases appear in the interdendritic areas. For the as-cast ERBOCo-0, the relatively high concentrations of Hf, Ti, and Ta in the interdendritic areas (EPMA measurement in Fig. 4) lets one expect the formation of intermetallic phases (structure map analysis in Fig. 6). Such precipitates were indeed identified experimentally in ERBOCo-0 [9], see Fig. 7 for a characteristic example.

The dark regions are surrounded by the  $\gamma'$  phase that appears as a continuous phase framing the precipitates. From the thermodynamic modelling in Ref. [9] one could expect the C14,  $\mu$ , B2, and  $D0_{24}$  phase to form. Here, using the Selected Area Diffraction (SAD) analysis the white precipitates could be identified as C14 Laves phases and the black regions as B2 phases by TEM diffraction patterns (Fig. 8c, e). A diffraction pattern of the needle-shaped precipitates (assigned to  $D0_{24}$  phases in Ref. [9]) could not be resolved. In higher-resolution HAADF STEM experiments (Fig. 8a) fairly sharp interfaces between  $\gamma'$ , B2, and C14-Laves phases were found. At the junction between the three phases (Fig. 8b) a small inclusion of an R-phase was identified (Fig. 8f).

The chemical compositions of the precipitates as obtained by EDS at the TEM [9] are compiled in Table 2, together with results of Scheil–Gulliver calculations discussed below. The corresponding positions in the structure map are indicated in Fig. 9.

The observed compositions are located within the corresponding phase stability region in the structure map (B2) or very close nearby (C14,  $D0_{24}$ ). The C14 phase exhibits local Co, Cr, and W concentrations close to the nominal composition. The Ni and Al concentrations in C14 are reduced, while the Ti, Ta, and Hf concentrations are

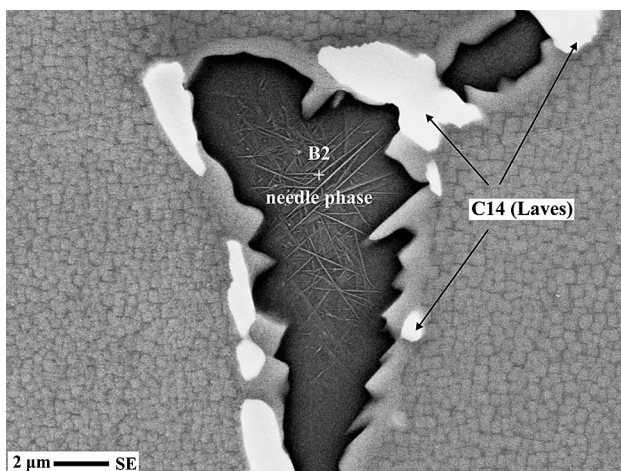


**Fig. 7** SEM (SE) micrograph of intermetallic precipitates in the  $\gamma/\gamma'$  microstructure of the dendritic area of as-cast ERBOCo-0

increased. These sizable local enrichments of early transition metals in the C14 precipitates effectively shifts the corresponding structure map position towards the stability region of the Laves phase (Fig. 9). The structure map analysis furthermore supports the identification of the needle-shaped precipitates as  $D0_{24}$  phases. The identified B2, Laves, and  $D0_{24}$  precipitates dissolve to a large extent in the homogenisation heat treatments [9]. The few remaining Laves phase precipitates undergo considerable changes in chemical composition [9] but remain within the Laves phase region in the structure map. This applicability of the structure map to precipitates in as-cast and heat-treated samples suggests that the local phase equilibrium plays an important role for TCP phases in superalloys.

### Solidification path modelling

The formation of secondary phases is also accessible through thermodynamic simulation of the solidification process. Here, CALPHAD calculations assuming Scheil solidification with the TCNi5 database were performed for ERBOCo-0 (see also Ref. [9]) and, for comparison, also for ERBO-1. For each temperature, the composition of the resulting phases was assigned to the SDP structure map in order to visualize the solidification path, see (Fig. 10). The CALPHAD calculations do not show any precipitation of  $\gamma'$  for ERBOCo-0, while they predict  $\gamma'$ -precipitation below 1310 °C for ERBO-1. In both cases, the precipitation of a  $\mu$  and B2 phase appears at a later state of solidification. Additionally, in ERBOCo-0 a Laves phase forms below 1180 °C and  $D0_{24}$  precipitation starts below 1000 °C. All predicted precipitate compositions are located within the corresponding phase stability regions in the structure map, except for the  $\mu$  phase in ERBO-1 that is just outside the  $\mu$  phase region. Such a slight deviation for multi-component  $\mu$ -phases has already been reported in Ref. [10]. In ERBO-1, all phases exhibit a tendency to a lower band filling as their composition changes during solidification. The same behaviour is also shown by the B2 and C14 phases in ERBOCo-0. The  $D0_{24}$  phase composition in ERBOCo-0 is constant at all stages of solidification. Hence, the corresponding solidification path in the structure map is only a single point (purple filled square in Fig. 10b). The solidification paths of the C14 and  $\mu$  phase show rapid changes due to sudden shifts in the band filling at  $T \approx 1060$  °C (C14) and  $T \approx 1050$  °C ( $\mu$ ). This is also reflected in the solidification path of the remaining liquid. In both alloys the composition of the remaining liquid at the end of the solidification is at lower  $\bar{N}$  and larger  $\Delta V/\bar{V}$  with respect to the nominal composition, i.e. closer to the region of the TCP phase stability. This is in line with the general trend of the EPMA results during solidification.

**Fig. 8** **a** STEM HAADF micrograph of the interfacial region between  $\gamma'$ , B2, and C14 Laves phase in as-cast ERBOCo-0. **b** Micrograph showing the area marked by the white rectangle **a** at higher magnification. **c–f** left characteristic SAD patterns taken from single-phase regions, right kinematic simulations obtained with JEMS software package [36]

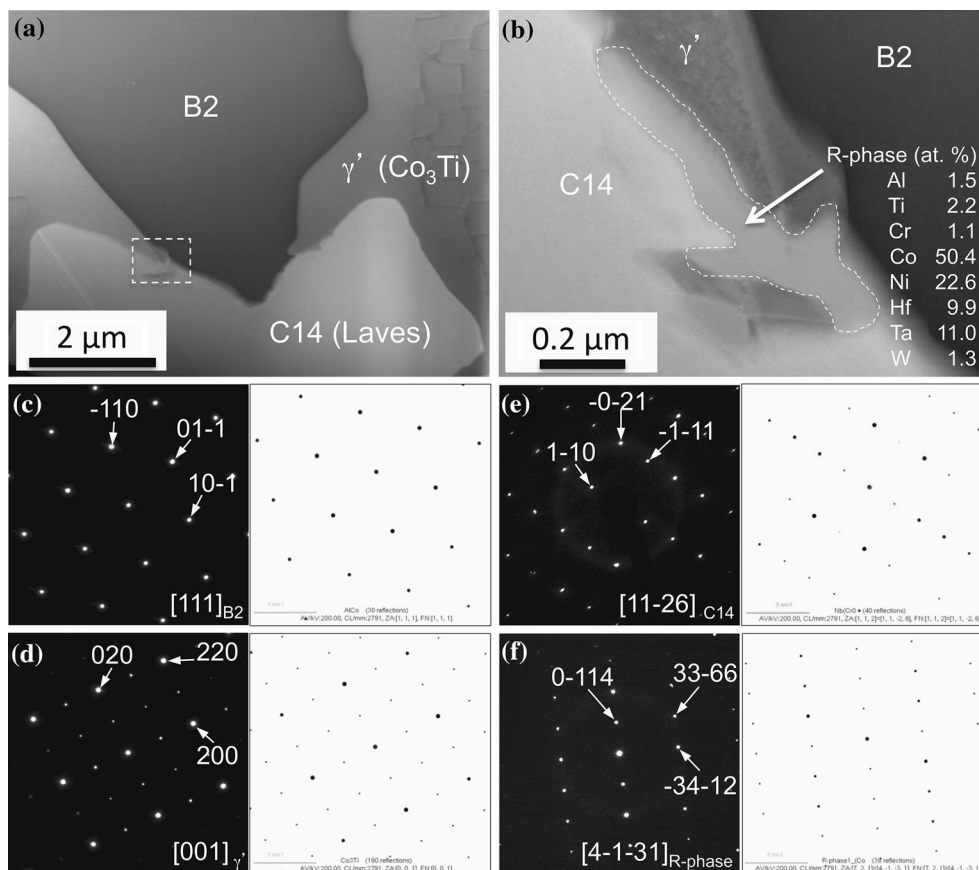


**Table 2** Composition of intermetallic phases at 975 °C in as-cast ERBOCo-0 (at.%) obtained by Scheil–Gulliver calculations and by TEM experiments [9] with corresponding structure map coordinates

		Fraction of alloying element (at.%)									Structure map	
		Ni	Co	Cr	W	Al	Ti	Ta	Hf	Si	$\bar{N}$	$\left(\frac{\Delta V}{V}\right)$
C14	Scheil	1.2	57.0	6.1	5.9	0.0	19.3	6.9	0.9	2.8	7.40	0.207
	TEM [9]	12.1	59.1	3.4	3.8	1.4	6.4	4.1	9.7	—	7.99	0.192
B2	Scheil	18.5	40.6	4.2	0.1	0.9	31.6	0.4	1.2	2.5	7.42	0.219
	TEM [9]	22.2	47.5	2.9	1.0	15.4	8.8	1.7	0.5	—	8.57	0.179
D0 <sub>24</sub>	Scheil	59.3	15.7	0.1	0.1	0.3	24.4	0.3	0.0	0.0	8.36	0.178
	TEM [9]	23.1	55.5	2.6	3.6	5.4	5.5	3.7	0.6	—	8.59	0.140
$\mu$	Scheil	2.0	46.1	12.7	39.2	0.0	0.0	0.0	0.0	0.0	7.46	0.169
	TEM	—Could not be identified in experiment—										

The predictions of the Scheil–Gulliver calculations are compared to the TEM results at 975 °C in Table 2 and in Fig. 9. The simulations reproduce the experimental observation of C14, D0<sub>24</sub>, and B2 phases, although with sizeable differences in chemical compositions. The Scheil–Gulliver results are shifted to smaller values of  $\bar{N}$ , particularly due to the significantly larger Ti concentration. The  $\mu$  phases predicted by the simulation could not be observed experimentally. This could be due to the as-cast state or the

limited application range of the TCNi5 database for this complex Co-based superalloy.

## Conclusions

In the current work, the microsegregation and precipitate formation of the multi-component Co-based superalloy ERBOCo-0 is characterized and compared to the ternary



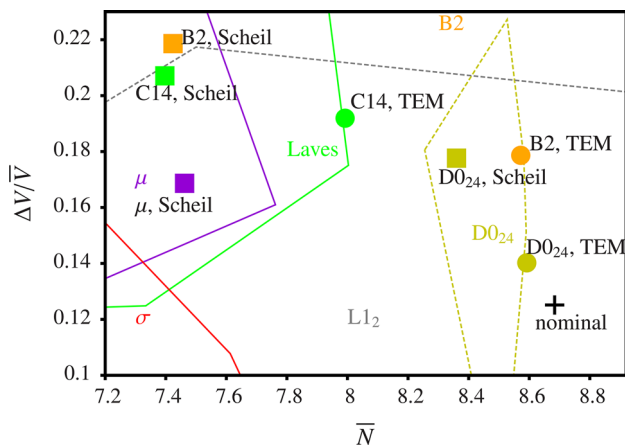


**Fig. 9** Structure map analysis of intermetallic precipitates in ERBOCo-0 at 975 °C. Chemical compositions obtained by TEM (circles) and Scheil–Gulliver calculations computation (squares) as given in Table 2

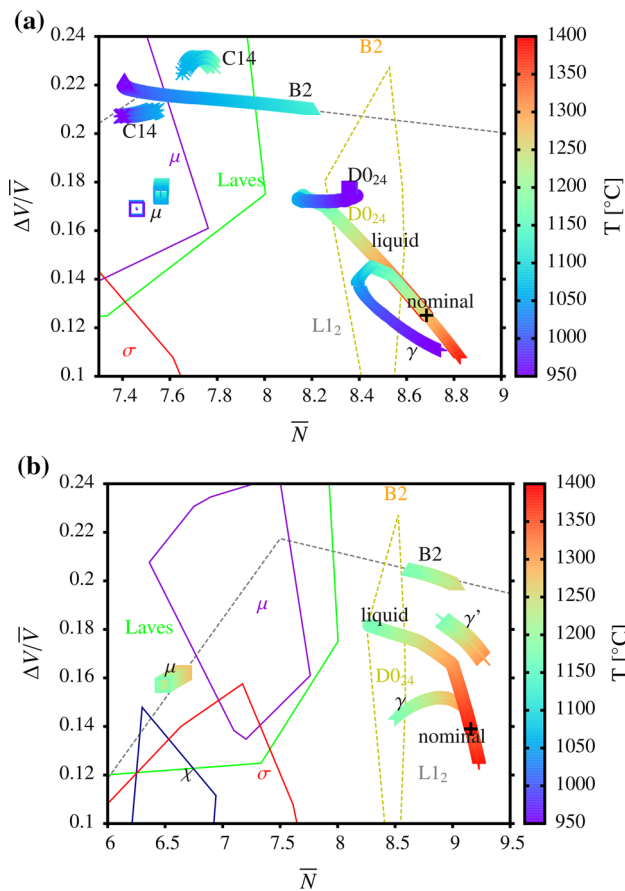


**Fig. 10** Structure map analysis of precipitation obtained by Scheil–Gulliver calculations for **a** ERBOCo-0 and **b** ERBO-1

ERBOCo-9W system and the Ni-based superalloys ASTRA-2W and ERBO-1. The experimental characterization of the as-cast microstructure (SEM, TEM, EDS) and the investigation of the elemental distribution during

solidification (EPMA) were combined with complementary theoretical descriptions of phase stability (structure map, CALPHAD).

EPMA measurements show that the microsegregation in the investigated Co-based and Ni-based superalloys is very similar. For the multi-component superalloys an enrichment of Co, Cr, and W in the dendrite cores and an enrichment of Ta, Ti, and Hf in the interdendritic regions were found. This trend is also observed in the corresponding segregation coefficients. In the ternary alloy ERBOCo-9W the microsegregation of W is weaker than in the multi-component systems while Co and Al behave similarly. The microsegregation coefficients for the individual elements are in general similar in the different Co-based and Ni-based superalloys. In ERBOCo-0 a strong microsegregation of Ta and Ti to the interdendritic region was observed that could counterbalance the microsegregation of W to the dendrite core and lead to a better castability compared to ERBO-1 and Astra2-W.

Plotting the EPMA results in terms of the structure map coordinates unites the individual elemental distributions in a physically motivated averaging scheme. The resulting microstructure maps for the compound provide a first estimate of potential locations of TCP phase precipitates in the microstructure. Furthermore, following the compositions along the solid fraction for ERBOCo-0, the structure map indicates that most local compositions are within the  $L1_2$  and B2 stability regions. Towards the end of the solidification process the compositions take values in the  $D0_{24}$ , Laves, and  $\mu$  phase regions.

The structure map analysis is confirmed by the experimental observation of several intermetallic precipitates. The B2 phase and the Laves phase C14 could be identified by TEM experiments, the latter with an enrichment of the early transition metals Ti, Ta, and Hf. Small inclusions of R-phase precipitates at the junction between the  $\gamma'$ , B2, and C14 were identified by TEM. Further needle-shaped precipitates are expected to be in  $D0_{24}$  phases. These findings are supported by CALPHAD-based solidification simulations using the TCNi5 database that also predict B2,  $D0_{24}$ , and C14 phase formation, although with considerable differences in chemical composition. The additional prediction of the  $\mu$  phase was not confirmed in our experiments. This can be due to the lack of time to reach thermodynamic equilibrium in the experiment or due to the limited applicability of the TCNi5 database in the simulations.

**Acknowledgements** We acknowledge financial support by the German Research Foundation (DFG) through projects A2, B3, B4, C1, and the service project WSP of the collaborative research center SFB/TR 103. We acknowledge Sabine Michel for performing the EPMA measurements and Katarzyna Matuszewska for performing single-crystal casting. JK, RD, and TH acknowledge financial support through ThyssenKrupp AG, Bayer MaterialScience AG, Salzgitter

Mannesmann Forschung GmbH, Robert Bosch GmbH, Benteler Stahl/Rohr GmbH, Bayer Technology Services GmbH, the state of North-Rhine Westphalia, the European Commission in the framework of the ERDF.

## References

- Rae C, Reed R (2001) The precipitation of topologically closed-packed phases in rhenium-containing superalloys. *Acta Mater.* 49:4113–4125
- Pollock T, Tin S (2006) Nickel-based superalloys for advanced turbine engines: Chemistry, microstructure, and properties. *J Propul Power* 22:361–374
- Sato J, Omori T, Ohnuma I, Kainuma R, Ishida K (2006) Cobalt-base high-temperature alloys. *Science* 312:90–91
- Suzuki A, DeNolf G, Pollock T (2007) Flow stress anomalies in  $\gamma/\gamma'$  two-phase Co-Al-W-base alloys. *Scripta Mater* 56:385–388
- Suzuki A, Pollock T (2008) High-temperature strength and deformation of  $\gamma/\gamma'$  two-phase Co-Al-W-base alloys. *Acta Mater.* 56:1288–1297
- Pollock T, Dibbern J, Tsunekane M, Zhu J, Suzuki A (2010) New Co-based  $\gamma - \gamma'$  high-temperature alloys. *JOM* 62:58–63
- Bauer A, Neumeier S, Pyczak F, Göken M (2010) Microstructure and creep strength of different  $\gamma/\gamma'$ -strengthened Co-base superalloy variants. *Scripta Mater* 63:1197–2000
- Bauer A, Neumeier S, Pyczak F, Singer R, Göken M (2012) Creep properties of different  $\gamma'$ -strengthened Co-base superalloys. *Mater Sci Eng* 550:333–341
- Lopez-Galilea I, Zenk C, Neumeier S, Huth S, Theisen W, Göken M (2014) The thermal stability of intermetallic compounds in an as-cast SX Co-base superalloy. *Advanced Engineering Materials*. (doi: 10.1002/adem.201400249)
- Seiser B, Drautz R, Pettifor D (2011a) TCP phase predictions in Ni-based superalloys: Structure maps revisited. *Acta Mater* 59:749–763
- Sinha A (1973) Topologically close-packed structures of transition metal alloys. *Prog Mat Sci* 15:79
- Darolia R, Lahrman D, Field R (1988) In: Reichman S, Duhl D, Maurer G, Antolovich S, Lund C (eds) *Superalloys 1988*, The Metallurgical Society, pp 255–264
- Rae C, Reed R (2001) The precipitation of topologically closed-packed phases in rhenium-containing superalloys. *Acta Mater* 49:4113–4125
- Pauling L (1947) Atomic radii and interatomic distances in metals. *J Am Chem Soc* 69:542–553
- Tilley R (2004) *Understanding solids: The science of materials*, 1st edn. Wiley&Sons
- Kaye G, Laby T (1993) *Tables of physical and chemical constants*, 15th edn. Longman, London, UK
- Porterfield W (1984) *Inorganic chemistry, a unified approach*. Addison Wesley Publishing Co., Reading Massachusetts, USA
- Berne C, Pasturel A, Sluiter M, Vinet B (1999) Ab initio study of metastability in refractory metal based systems. *Phys Rev Lett* 83:1621
- Berne C, Sluiter M, Pasturel A (2002) Theoretical approach of phase selection in refractory metals and alloys. *J Alloys Comp* 334:27
- Turchi PEA (1991) Interplay between local environment effect and electronic structure properties in close packed structures. *Mat Res Soc Symp Proc* 206:265
- Hammerschmidt T, Seiser B, Drautz R, Pettifor DG (2008) Modelling topologically close-packed phases in superalloys: Valence-dependent bond-order potentials based on ab-initio calculations. In: Reed RC, Green K, Caron P, Gabb T, Fahrman M, Huron E, Woodward S (eds) *Superalloys 2008*. Minerals and Materials Society, The Metals, p 847
- Seiser B, Hammerschmidt T, Kolmogorov AN, Drautz R, Pettifor DG (2011b) Theory of structural trends within 4d and 5d transition metals topologically close-packed phases. *Phys Rev B* 83(224):116
- Hammerschmidt T, Seiser B, Cak M, Drautz R, Pettifor DG (2012) Structural trends of topologically close-packed phases: Understanding experimental trends in terms of the electronic structure. In: Huron ES, Reed RC, Hardy MC, Mills MJ, Montero RE, Portella PD, Telesman J (eds) *Superalloys 2012*. Minerals and Materials Society, The Metals, pp 135–142
- Hammerschmidt T, Bialon AF, Pettifor DG, Drautz R (2013) Topologically close-packed phases in binary transition-metal compounds: matching high-throughput ab-initio calculations to an empirical structure-map. *New J Phys* 15(115):016
- Villars P, Cenzual K (2012/13) *Pearson's crystal data – crystal structure database for inorganic compounds (on CD-ROM)*. ASM International, Materials Park, Ohio, USA
- Lukas H, Fries S, Sundman B (2007) *Computational Thermodynamics: The CALPHAD Method*. Cambridge University
- Spencer P (2008) A brief history CALPHAD. *CALPHAD* 32:1–8
- Andersson J, Helander T, Höglund L, Shi P, Sundman B (2002) Thermo-Calc and DICTRA, computational tools for materials science. *Calphad* 26:273–312
- Thermo-Calc Software TCNi5 Ni-based Superalloys Database, Version 5.0, URL: <http://www.thermocalc.com>
- Gungor M (1989) A statistically significant experimental technique for investigating microsegregation in cast alloys. *METALL TRANS A* 20:2529–2533
- Karunaratne M, Cox D, Carter P, Reed R (2000) Modelling of the microsegregation in CMSX-4 superalloy and its homogenisation during heat treatment. *Superalloys 2000*:263–273
- Tsunekane M, Suzuki A, Pollock T (2011) Single-crystal solidification of new Co-Al-W base alloys. *Intermetallics* 19:636–643
- Hobbs R, Tin S, Rae C, Broomfield R, Humphreys C (2004) Solidification characteristics of advanced nickel-base single crystal superalloys. *Superalloys 2004*:819–825
- Kearsey R, Beddoes J, Jones P, Au P (2004) Compositional design considerations for microsegregation in single crystal superalloy systems. *Intermetallics* 12:903–910
- Tin S, Pollock T (2003) Stabilization of thermosolutal convective instabilities in Ni-based single-crystal superalloys. *Metall Mater Trans A* 34A:1953–1967
- Stadelmann P.A. (2004), JEMS-EMS java version, version 3.8